Algorithm Design for Femtocell Base Station Placement in Commercial Building Environments

Jia Liu* Qian Chen† Hanif D. Sherali‡
* Department of Electrical and Computer Engineering, The Ohio State University, Columbus, OH 43210
† Construction Systems Management, The Ohio State University, Columbus, OH 43210
‡ Grado Department of Industrial and Systems Engineering, Virginia Tech, Blacksburg, VA 24061

***Abstract*—Although femtocell deployments in residential buildings have been increasingly prevalent, femtocell deployment in commercial building environments remains in its infancy. One of the main challenges lies in the femtocell base stations (FBS) placement problem, which is complicated by the buildings' size, layout, structure, and floor/wall separations. In this paper, we investigate a joint FBS placement and power control optimization problem in commercial buildings with the aim to prolong mobile handsets' battery lives. We first construct a mathematical model that takes into account the unique floor attenuation factor (FAF) and FBS installation restrictions in building environments. Based on this model, we propose a novel two-step reformulation approach to convert the original mixed-integer nonconvex problem (MINCP) into a mixed-integer linear program (MILP), which enables the design of efficient global optimization algorithms. We then devise a global optimization algorithm by utilizing the MILP in a branch-and-bound framework. This approach guarantees finding a global optimal solution. We conduct extensive numerical studies to demonstrate the efficacy of the proposed algorithm. Our mathematical reformulation techniques and optimization algorithm offer useful theoretical insights and valuable tools for future commercial building femtocell deployments.**

I. Introduction

Studies on wireless usage show that, as smartphones, tablets, and other data intensive mobile devices continue to proliferate, more than 50 percent of all voice calls and more than 70 percent of data traffic originate from indoors [1]. Accordingly, recent years have witnessed increasing acceptance of femtocell systems as an important means to extend and improve network coverage in building environments. Simply speaking, femtocells are low-cost, small-sized base stations that offer high quality voice/data services to indoor users. As a result, not only can indoor users enjoy better network coverage, the operators also benefit from huge savings due to a reduced demand for constructing macrocell towers. This "win-win" situation has sparked a great deal of interests in many femtocell research topics, such as local area coverage [2], [3], synchronization and interference management [4], [5], [6], self-organization/configuration [7], [8], and access and quality-of-service (QoS) control [9], [10], just to name a few. Also, WCDMA, LTE, and WiMAX femtocells are being standardized by 3GPP, 3GPP2, and WiMAX Forum (IEEE 802.16), respectively [11], [12]. Meanwhile, residential femtocell deployments have been commercially launched by more than a dozen major operators worldwide [13].

While residential deployments have clearly positioned femtocells as an enabling technology for future wireless communications, it is expected that the next wave of femtocell deployment will target commercial building environments (e.g., large enterprises, big-box stores, dormitories, malls, airports, and other public places) [13]. However, research progress in this area remains rather limited. In particular, femtocell base stations (FBS) placement problems have been largely overlooked in commercial buildings. The need for femtocell placement optimization is compelling due to the following two reasons. First, the location of an FBS has a high impact on the *energy expenditure* of each mobile handset (HS) under its coverage. It is well-known that the uplink transmit power of an HS depends heavily on the physical distance and obstructions between the HS and its targeted FBS. Second, the battery performance of current smartphone devices is far from satisfactory (less than eight hours even under moderate use [14], [15]). Increasing battery capacity proves to be difficult because it is fundamentally limited by advances in material sciences. As a result, FBS placement optimization becomes one of the most effective ways to address the battery life issue of mobile handsets.

However, FBS placement problems in commercial buildings are challenging. Unlike small-sized residential buildings, commercial buildings range from small offices to large-sized structures with different building layouts (e.g., open atriums, contained offices, hallways, or basements) with various floor and wall separations, which yield complex signal path loss models and may require multiple FBSs. Also, there could be special building safety codes/constraints that impose further restrictions on the FBS locations. Due to the lack of results in this area, the main objective of this work is to fill this gap and to obtain a fundamental understanding of the FBS placement problem in commercial building environments.

More specifically, in this paper, we focus on the joint optimization of FBS placement to minimize the uplink transmission power of each mobile HS, while ensuring network coverage and meeting each HS's QoS requirement. The main contributions of this work are as follows:

- We construct a tractable mathematical model for joint FBS placement and power control optimization in commercial building environments. Our model takes into account the unique floor attenuation factor (FAF) and FBS installation restrictions in buildings.
- Based on the proposed model, we show that the joint

FBS placement and power control optimization problem is a challenging *mixed-integer nonconvex programming* problem (MINCP), for which no existing optimization methods can be readily applied. To address the nonconvexity and integrality difficulty, we propose a novel *two-step reformulation approach* to transform the original MINCP into an equivalent *mixed-integer convex program* (MICP) and then into a *mixed-integer linear program* (MILP). This two-step reformulation enables the design of efficient global optimization algorithms.

- For the reformulated MILP problem, we propose a global optimization approach that utilizes its linear relaxation within a branch-and-bound framework, which *guarantees* finding a global optimal solution. To demonstrate the efficacy of our algorithmic procedures, we conduct extensive computational studies. Our proposed modeling and mathematical optimization approaches offer useful theoretical insights and practical tools for femtocell deployments in commercial buildings.

The remainder of this paper is organized as follows. We introduce our network model and problem formulation in Section II. Section III and Section IV present the key components of our proposed two-step reformulation approach. Then, a solution procedure based on the branch-and-bound framework using linear programming relaxations is presented in Section V. Numerical results are presented in Section VI, and Section VII concludes this paper with a summary and recommendations for future research.

II. Network Model and Problem Formulation

A. Network Model

We consider a femtocell network in a commercial building with M FBSs. Here, we assume that M is large enough to ensure network coverage. More detailed discussions on the minimum required M can be found in Section V. To model the random distribution of the mobile HS, we partition the building into subregions and associate each subregion with an "occupant probability," as shown in Fig. 1. More specifically, we partition the length and width of the building into L and W units, respectively. Also, we let F denote the maximum number of floors. Then, each subregion can be indexed by a three-tuple (i, j, k), $i = 1, \ldots, L$, $j = 1, \ldots, W$, and $k = 1, \ldots, F$. The occupant probability of subregion (i, j, k) is denoted by $q_{ijk} \in [0, 1]$, where

$$\sum_{i=1}^{L} \sum_{j=1}^{W} \sum_{k=1}^{F} q_{ijk} = 1. \tag{1}$$

We index the FBSs as FBS 1, ..., FBS M. We assume that the femtocell-to-femtocell and femtocell-to-macrocell interferences (including femtocell leakage [8]) are negligible under some appropriate channel assignment/spectral management schemes. There has been a large body of literature on femtocell interference management (see, e.g., [4], [5], [6] and references therein) and its discussion is beyond the scope of this paper.

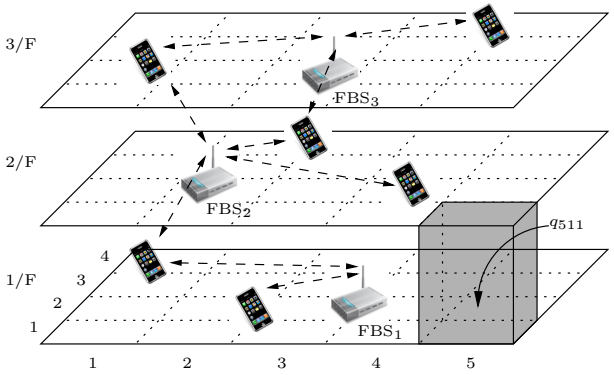

Fig. 1. An illustration of a femtocell network with multiple FBSs and HSs in a multi-floor commercial building. The building is partitioned into a set of subregions, each of which is associated with an occupant probability.

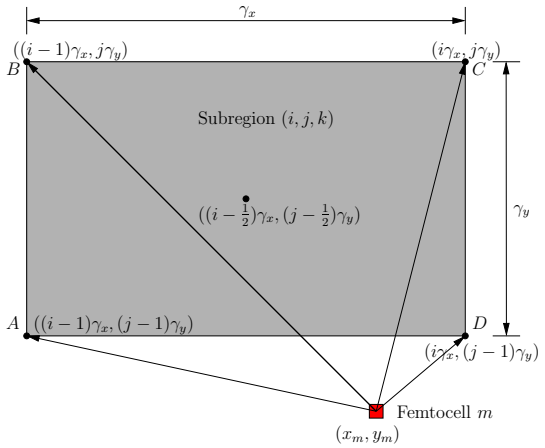

Fig. 2. The horizontal distance projection between FBS m and subregion (i, j, k).

Next, we derive the distance relationship between an FBS and a subregion, which is more complex than the conventional Euclidean distance due to the unique features in building environments. First, since commercial buildings usually have multiple floors, the coordinates of FBSs and HSs are in 3-D space. We use (x_m, y_m, z_m), $m = 1, \ldots, M$, to denote the coordinates of the m-th FBS, which are to be optimized. Also, we let γ_x and γ_y denote the length and width of each subregion: $\gamma_x = \frac{1}{L} x_{\max}$ and $\gamma_y = \frac{1}{W} y_{\max}$, where $x_{\max}$ and $y_{\max}$ denote the entire length and width of the building, respectively.

We first consider the horizontal distance between FBS m and subregion (i, j, k), as shown in Fig. 2. For an FBS to cover every point in a subregion, the horizontal distance projection between FBS m and subregion (i, j, k) is defined as the distance between the FBS and the point in the subregion that is *furthest* away from FBS m. For example, in Fig. 2, the point in subregion (i, j, k) furthest away from FBS m is point B. It is not difficult to verify that, in general, the x-axis and y-axis projections of horizontal distance are $|x_m - (i - \frac{1}{2})\gamma_x| + \frac{1}{2}\gamma_x$ and $|y_m - (j - \frac{1}{2})\gamma_y| + \frac{1}{2}\gamma_y$, respectively.

Next, we consider the vertical distance. Due to the practical use of building space, FBSs are usually required to be mounted

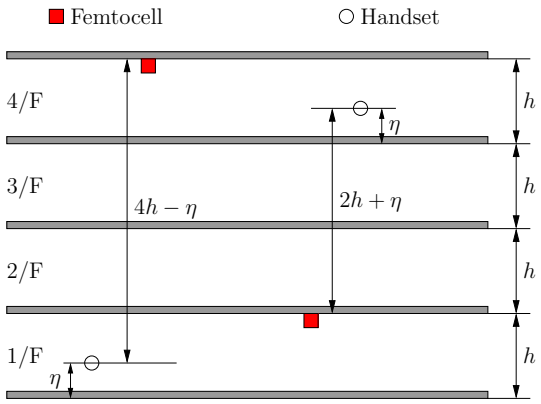

Fig. 3. The vertical distances between femtocell base stations and handsets.

on the ceiling of each floor to avoid being obstructions. To model this, we restrict the vertical coordinates z_m to be integer-valued and in the set $\{1, 2, \ldots, F\}$. For example, $z_m = 3$ represents that FBS m is on the ceiling of the third floor. Also, in reality, the HSs in each subregion are approximately three to four feet above the ground of each floor because of the average human height. Thus, we let η denote the average height of an HS on each floor. We assume that the height of each floor is h. Then, the vertical distance can be computed as $|(z_m - k + 1)h - \eta|$. To verify the correctness in the vertical direction, see the example as shown in Fig. 3. If the FBS is on the fourth floor and the HS is on the first floor, we have $|(4 - 1 + 1)h - \eta| = 4h - \eta$. On the other hand, if the FBS is on the first floor and the HS is on the fourth floor, we have $|(1 - 4 + 1)h - \eta| = 2h + \eta$.

Combining the horizontal and vertical distance projections, the distance between FBS m and subregion (i, j, k), denoted by $d_{ijk}^{(m)}$, can be computed as

$$d_{ijk}^{(m)} = \Big[(|x_m - (i - \frac{1}{2})\gamma_x| + \frac{1}{2}\gamma_x)^2 + (|y_m - (j - \frac{1}{2})\gamma_y| + \frac{1}{2}\gamma_y)^2 + |(z_m - k + 1)h - \eta|^2\Big]^{\frac{1}{2}},$$

where $i = 1, \ldots, L$, $j = 1, \ldots, W$, $k = 1, \ldots, F$, and $m = 1, \ldots, M$. Also, we let P_{ijk} denote the uplink transmission power of HSs in subregion (i, j, k). Due to the transceiver hardware constraint, the transmission power of an HS cannot exceed a certain upper limit. This can be modeled as $0 \leq P_{ijk} \leq P_{\max}$, $\forall i, j, k$, where $P_{\max}$ denotes the maximum transmission power limit for the HS.

B. Wireless Signal Path Loss Modeling for Commercial Buildings

Since wall separations vary from one building to another in commercial building environments, it is in general intractable to account for every wall separation loss in path loss modeling within the same floor. To address this difficulty, we adopt the following equation to model path loss (in dBm) [16] within the same floor:

$$P_r = P_t - L_{d_0} - 10\alpha \log_{10}\left(\frac{d}{d_0}\right) + \zeta_\sigma, \quad (2)$$

where P_t and P_r are the transmission and received powers, d represents the distance, α denotes the path loss exponent, d_0 is a short reference distance from the transmitter, and L_{d_0} represents the loss (dB) of signal for the reference distance d_0. In (2), ζ_σ is a zero-mean Gaussian random variable with standard deviation σ, which models the log-normal shadowing effect of path loss [16]. Since extensive measurement experiments have been conducted to determine α for a large number of partition types (see [16, Table 4.3]), this allows us to use different values of α to model different buildings.

To incorporate the path loss between different floors, the path loss model in (2) can be further augmented as [16]:

$$P_r = P_t - L_{d_0} - 10\alpha \log_{10}\left(\frac{d}{d_0}\right) + \zeta_\sigma - L_{FAF}, \quad (3)$$

where L_{FAF} (in dB) denotes the path loss due to floor attenuation factor (FAF), and where FAF is determined by the external dimensions and materials of the building, as well as by the type of construction methods used for the floors and the external surroundings [17], [18], [16]. Moreover, the FAF can be modeled as (in dB) [16]:

$$L_{FAF} = \begin{cases} \Delta_1 + (\varphi - 1)\Delta_a, & \text{if } \varphi \geq 1, \\ 0, & \text{if } \varphi = 0, \end{cases} \quad (4)$$

where Δ_1 represents the FAF for a single floor separation, Δ_a represents the FAF for each additional floor, and φ denotes the number of separating floors.

Ignoring ζ_σ for now and converting Eq. (3) to a linear scale, we have the following result (due to limited space, we refer readers to [19, Appendix A] for details of the proof).

Lemma 1. *Denote P_{ijk} and P_{R_m} as the transmission and received power levels for the transmission between subregion (i, j, k) and FBS m, respectively. Then, under the wireless signal path loss model in commercial building environments and upon converting P_{R_m}, P_{ijk}, and L_{d_0} to a suitable linear scale, the following relationship holds between P_{ijk} and P_{R_m}:*

$$P_{R_m} = \frac{P_{ijk}}{C(z_m, k)(d_{ijk}^{(m)})^\alpha \Delta^{|z_m - k|}}, \quad \forall m = 1, \ldots, M, \quad (5)$$

where Δ is a constant that depends on the specific environment; $C(z_m, k)$ is a step function that depends on z_m and k and has the following structure:

$$C(z_m, k) = \begin{cases} C_0, & \text{if } z_m = k, \\ C_1, & \text{if } z_m \neq k, \end{cases}$$

where C_0 and C_1 are constants that also depend on the specific environment.

C. QoS Requirement Constraints

To reliably decode an HS's transmission from subregion (i, j, k) at a data rate that satisfies the HS's rate requirement, it is necessary that the uplink received power level at the FBS should be above a certain threshold value. Let $P_{\min}$ denote the minimum power level (in dB). According to (3), the received power is Gaussian (in dB). Hence, we use outage probability as the QoS requirement, defined as $\Pr\{P_r < P_{\min}\}$, where we

require this quantity to be less than or equal to a target value β, i.e.,

$$\Pr\left\{P_t - L_{d_0} - 10\alpha\log_{10}\left(\frac{d}{d_0}\right) + \zeta_\sigma - L_{FAF} < P_{\min}\right\} \le \beta.$$

For convenience, we let $\bar{P} \triangleq P_t - L_{d_0} - 10\alpha\log_{10}\left(\frac{d}{d_0}\right) - L_{FAF}$. Then, the above equation can be rewritten as:

$$\Pr\left\{\frac{P_r - \bar{P}_r}{\sigma} < \frac{P_{\min} - \bar{P}_r}{\sigma}\right\} \le \beta. \quad (6)$$

Note that $\frac{P_r - \bar{P}_r}{\sigma}$ is a standard normal random variable. Hence, the probability in (6) is simply $\Phi(\frac{P_{\min} - \bar{P}_r}{\sigma})$, where $\Phi(x) = \frac{1}{\sqrt{2\pi}}\int_{-\infty}^{x} e^{-\frac{t^2}{2}}dt$ is the cumulative distribution function (cdf) of the standard normal distribution. Thus, the outage probability constraint in (6) can be written as $\frac{P_{\min} - \bar{P}_r}{\sigma} \le \Phi^{-1}(\beta)$, which in turn yields $\bar{P}_r \ge P_{\min} - \sigma\Phi^{-1}(\beta)$. Letting $P_{\min}^{(\sigma,\beta)} \triangleq P_{\min} - \sigma\Phi^{-1}(\beta)$, we can obtain (in dB):

$$P_t - L_{d_0} - 10\alpha\log_{10}\left(\frac{d}{d_0}\right) - L_{FAF} \ge P_{\min}^{(\sigma,\beta)}. \quad (7)$$

Further, based on the path loss model in Lemma 1, we have (in linear scale)

$$\frac{P_{ijk}}{C(z_m,k)(d_{ijk}^{(m)})^\alpha \Delta^{|z_m-k|}} \ge P_{\min}^{(\sigma,\beta)}, \quad \forall i,j,k,m. \quad (8)$$

By rearranging terms and letting $A(z_m,k) \triangleq C(z_m,k)P_{\min}^{(\sigma,\beta)} = \begin{cases} A_0 \triangleq C_0 P_{\min}^{(\sigma,\beta)} & \text{if } z_m = k, \\ A_1 \triangleq C_1 P_{\min}^{(\sigma,\beta)} & \text{if } z_m \ne k, \end{cases}$ we can rewrite the QoS constraint in (8) as

$$A(z_m,k)(d_{ijk}^{(m)})^\alpha \Delta^{|z_m-k|} - P_{ijk} \le 0, \ \forall i,j,k,m. \quad (9)$$

D. FBS Association Modeling

Unlike conventional wireless networks, the channel to the nearest FBS may not be the best for a given subregion. This is because the closest FBS could be separated by a floor and hence could lead to a worse path loss due to FAF. Therefore, we try not to define a specific rule for FBS association. Instead, we model the FBS association problem as a part of the overall joint FBS placement and power control optimization problem. To this end, we first define the following binary variables:

$$\pi_{ijk}^{(m)} = \begin{cases} 1 & \text{if subregion } (i,j,k) \text{ is associated with FBS } m, \\ 0 & \text{otherwise.} \end{cases} \quad (10)$$

Then, the FBS association can be modeled as

$$\sum_{m=1}^{M} \pi_{ijk}^{(m)} = 1, \quad \forall i,j,k. \quad (11)$$

Also, we need to modify the QoS constraints in (9) as follows:

$$A(z_m,w)\pi_{ijk}^{(m)}(d_{ijk}^{(m)})^\alpha \Delta^{|z_i-w|} - P_{ijk} \le 0, \quad \forall i,j,k,m. \quad (12)$$

Hence, if $\pi_{ijk}^{(m)} = 1$, then (12) is identical to the original QoS constraint in (9). Otherwise, (12) reduces to $P_{ijk} \ge 0$, which is trivially valid.

E. Problem Formulation

To reduce energy consumption and ensure fairness among the HSs, our goal is to minimize the power consumption of the HS in the subregion that transmits at the highest weighted power level (weighted by occupant probability), i.e., $\min\{\max_{i,j,k}(q_{ijk}P_{ijk})\}$. For easier manipulation, we rewrite the minimax objective function in an equivalent form as $\min P$, subject to $P \ge q_{ijk}P_{ijk}, \forall i,j,k$. Incorporating other constraints established earlier, we can formulate the joint FBS placement and power control problem (FPPC) as follows:

FPPC:

$$\text{Min.} \quad P \quad (13)$$

$$\text{s.t.} \quad P \ge q_{ijk}P_{ijk}, \quad \forall i,j,k, \quad (14)$$

$$A(z_m,k)\pi_{ijk}^{(m)}(d_{ijk}^{(m)})^\alpha \Delta^{|z_i-k|} - P_{ijk} \le 0, \quad \forall i,j,k,m, \quad (15)$$

$$\sum_{m=1}^{M} \pi_{ijk}^{(m)} = 1, \quad \forall i,j,k, \quad (16)$$

$$d_{ijk}^{(m)} = \big[(|x_m - (i-\frac{1}{2})\gamma_x| + \frac{1}{2}\gamma_x)^2 + (|y_m - (j-\frac{1}{2})\gamma_y| + \frac{1}{2}\gamma_y)^2 + |(z_m - k + 1)h - \eta|^2\big]^{\frac{1}{2}}, \quad \forall i,j,k,m, \quad (17)$$

$$0 \le P_{ijk} \le P_{\max}, \pi_{ijk}^{(m)} \text{ binary } \forall i,j,k,m,$$

$$0 \le x_m \le x_{\max},\ 0 \le y_m \le y_{\max},\ \forall m,$$

$$1 \le z_m \le F,\ \forall m,\ z_m \text{ binary},$$

where the decision variables are $[x_m, y_m, z_m]^T$, $d_{ijk}^{(m)}$, P_{ijk}, and $\pi_{ijk}^{(m)}$, $\forall i,j,k,m$.

Since FPPC involves integer variables $\pi_{ijk}^{(m)}$ and z_m along with nonconvex constraints in (15) and (17), this problem is a *mixed-integer nonconvex problem*, which is NP-hard in general [20]. Also, since (15) is highly unstructured, directly solving FPPC is difficult and no standard optimization tools can be readily applied. In the next two sections, we employ a novel two-step reformulation approach to transform FPPC into a mixed-integer linear program, which is much easier to handle. Then, we propose a global optimization approach that guarantees finding an optimal solution of the reformulated problem.

III. Reformulation Step One: From Nonconvex Modeling to Convex Modeling

Note that the difficulty in solving Problem FPPC stems from the term $A(z_m,k)\pi_{ijk}^{(m)}(d_{ijk}^{(m)})^\alpha\Delta^{|z_m-k|}$ in (15) and the nonconvexity in (17). Hence, our goal in this section is to convexify the highly unstructured constraint (15) and the nonconvex constraint in (17).

Reformulating the Distance Constraint in (17): We start by manipulating the relatively simpler constraint (17). We first let $\delta_{ijk}^{(m)} \triangleq (d_{ijk}^{(m)})^2$, $\forall i,j,k,m$, so that the constraint in (17)

can be rewritten as

$$\delta_{ijk}^{(m)} = (|x_m-(i-\frac{1}{2})\gamma_x|+\frac{1}{2}\gamma_x)^2+(|y_m-(j-\frac{1}{2})\gamma_y|+\frac{1}{2}\gamma_y)^2 + ((z_m-k+1)h-\eta)^2, \quad \forall i,j,k,m. \quad (18)$$

Accordingly, (15) becomes:

$$A(z_m,k)\pi_{ijk}^{(m)}(\delta_{ijk}^{(m)})^{\frac{\alpha}{2}}\Delta^{|z_i-k|} - P_{ijk} \leq 0. \quad (19)$$

Then, we have the following result:

Lemma 2. *The constraint in (18) can be equivalently replaced by*

$$(|x_m-(i-\frac{1}{2})\gamma_x|+\frac{1}{2}\gamma_x)^2+(|y_m-(j-\frac{1}{2})\gamma_y|+\frac{1}{2}\gamma_y)^2+ ((z_m-k+1)h-\eta)^2-\delta_{ijk}^{(m)} \leq 0, \quad \forall i,j,k,m. \quad (20)$$

Moreover, the inequality in (20) automatically holds as an equality at an optimal solution.

Proof: Consider Problem FPPC with (15) and (17) respectively replaced by (19) and (20), and suppose that (20) holds as a strict inequality at optimality for some i,j,k,m. Then, by decreasing the values of $\delta_{ijk}^{(m)}$ to make (20) hold as an equality, we still maintain feasibility in (19), and hence retain the optimality of the revised solution. ■

It is not difficult to verify that (20) is convex. However, we note that the left-hand-side of (20) involves absolute values, which are non-differentiable and remains cumbersome for designing optimization algorithms. To address this issue, we let $X_{mi} \triangleq |x_m-(i-\frac{1}{2})\gamma_x|$ and $Y_{mj} \triangleq |y_m-(j-\frac{1}{2})\gamma_y|$. Then, Eq. (20) can be rewritten as the following group of constraints:

$$\begin{cases} (X_{mi}+\frac{1}{2}\gamma_x)^2+(Y_{mj}+\frac{1}{2}\gamma_y)^2+ \\ \quad (hz_m-((k-1)h+\eta))^2-\delta_{ijk}^{(m)} \leq 0, \\ |x_m-(i-\frac{1}{2})\gamma_x| = X_{mi}, \quad |y_m-(j-\frac{1}{2})\gamma_x| = Y_{mj}. \end{cases} \quad (21)$$

It can be seen in (21) that the first constraint is a quadratic convex constraint. Next, we rewrite the second constraint as follows: $|x_m-(i-\frac{1}{2})\gamma_x| \leq X_{mi}$, which is based on the same argument as in Lemma 2. This can be further linearized as $x_m-(i-\frac{1}{2})\gamma_x \leq X_{mi}$ and $-x_m+(i-\frac{1}{2})\gamma_x \leq X_{mi}$. The third constraint can also be rewritten in the same fashion. After rearranging terms, we arrive at the following result:

Lemma 3. *The distance constraint (17) can be convexified as:*

$$(X_{mi}+\frac{1}{2}\gamma_x)^2+(Y_{mj}+\frac{1}{2}\gamma_y)^2+ (hz_m-((k-1)h+\eta))^2-\delta_{ijk}^{(m)} \leq 0, \quad (22)$$

$$x_m - X_{mi} \leq (i-\frac{1}{2})\gamma_x, \text{ and } x_m+X_{mi} \geq (i-\frac{1}{2})\gamma_x, \quad (23)$$

$$y_m - Y_{mj} \leq (j-\frac{1}{2})\gamma_y, \text{ and } y_m+Y_{mj} \geq (j-\frac{1}{2})\gamma_y. \quad (24)$$

Reformulating the Minimum Received Power Constraint in (15): Next, we reformulate constraint (15), which is more involved than (17). Recall that we have restated (15) as (19) by the change of variables. We now *linearize* (19) with respect to the binary variables $\pi_{ijk}^{(m)}$, which leads to the following result:

Lemma 4. *Constraint (15) is equivalent to the following alternative representation:*

$$A(z_m,k)(\delta_{ijk}^{(m)})^{\frac{\alpha}{2}}\Delta^{|z_m-k|} - (1-\pi_{ijk}^{(m)})U_{ijk}^{(m)} - P_{ijk} \leq 0, \forall i,j,k,m, \quad (25)$$

where $U_{ijk}^{(m)}$ is some upper bound for $A(z_m,k)(\delta_{ijk}^{(m)})^{\frac{\alpha}{2}}\Delta^{|z_m-k|}$.

Lemma 4 can be easily proven by considering $\pi_{ijk}^{(m)} \in \{0,1\}$, and verifying the logical equivalence between (25) and (19). In Lemma 4, a valid value for the upper bound $U_{ijk}^{(m)}$ can be chosen as

$$U_{ijk}^{(m)} \triangleq P_{\min}^{\sigma,\beta}\max\{C_0,C_1\}(\bar{\delta}_{ijk})^{\frac{\alpha}{2}}\Delta^{\max\{k-1,F-k\}},$$

where $\bar{\delta}_{ijk}$ is an upper bound for $\delta_{ijk}^{(m)}$. Recall that $x_{\max}$ and $y_{\max}$ denote the length and width of the building, respectively. Then, $\bar{\delta}_{ijk}$ can be computed as

$$\begin{aligned}\bar{\delta}_{ijk} &= \max\{(i\gamma_x)^2,(L-i+1)^2\gamma_x^2\} \\ &\quad + \max\{(j\gamma_y)^2,(W-j+1)^2\gamma_y^2\} \\ &\quad + \max\{((2-k)h-\eta)^2,((F-k+1)h-\eta)^2\}.\end{aligned}$$

Next, to further simplify the nonconvex constraint (25), we introduce two new variables $\nu_{ijk}^{(m)} \triangleq (\delta_{ijk}^{(m)})^{\frac{\alpha}{2}}$ and $\mu_{mk} \triangleq \Delta^{|z_m-k|}$ and rewrite (25) as the following three *simpler* nonconvex constraints:

$$\begin{cases} A(z_m,k)\nu_{ijk}^{(m)}\mu_{mk}- \\ \qquad (1-\pi_{ijk}^{(m)})U_{ijk}^{(m)} - P_{ijk} \leq 0, \forall i,j,k,m, \\ \nu_{ijk}^{(m)} = (\delta_{ijk}^{(m)})^{\frac{\alpha}{2}}, \quad \forall i,j,k,m, \\ \mu_{mk} = \Delta^{|z_m-k|}, \quad \forall m,k. \end{cases} \quad (26)$$

Now, the reformulation task of (15) boils down to convexifying these three nonconvex constraints. First, consider the nonconvex constraint $\nu_{ijk}^{(m)} = (\delta_{ijk}^{(m)})^{\frac{\alpha}{2}}$ in (26). Following the same approach as in Lemma 2, we can rewrite this as:

$$\nu_{ijk}^{(m)} \geq (\delta_{ijk}^{(m)})^{\frac{\alpha}{2}}, \quad \forall i,j,k,m. \quad (27)$$

Note that the inequality constraint in (27) is now convex since the path loss exponent α is greater than 2 in practice.

To simplify and convexify the remaining two nonconvex constraints in (26), we first employ the following trick to represent the general integer variable z_m via 0–1 variables:

$$z_m = \sum_{l=1}^{F} l\lambda_{ml}, \quad \forall m, \quad (28)$$

and

$$\sum_{l=1}^{F}\lambda_{ml} = 1, \quad \forall m, \quad (29)$$

where all λ_{ml}–variables are binary (i.e., $\lambda_{ml} \in \{0,1\}$). Using (28), it is clear that the third nonconvex constraint in (26) (i.e., $\mu_{mk} = \Delta^{|z_m - k|}$) is *logically equivalent to*

$$\mu_{mk} = \sum_{l=1}^{F} \lambda_{ml} \Delta^{|l-k|}, \tag{30}$$

which is *linear* with respect to λ_{ml}–variables (because all the $\Delta^{|l-k|}$-values are constants). Based on this alternative representation of μ_{mk}, we have the following result for convexifying the first constraint in (26) (see [19, Appendix B] for details of the proof):

Lemma 5. *Let $g_{ijk}^{(ml)} \triangleq \nu_{ijk}^{(m)} \lambda_{ml}$. Then, the first constraint in (26) can be linearized as*

$$A_1 \sum_{l=1, l\neq k}^{F} \Delta^{|l-k|} g_{ijk}^{(ml)} + A_0 g_{ijk}^{(mk)} - (1 - \pi_{ijk}^{(m)}) U_{ijk}^{(m)} - P_{ijk} \leq 0, \ \forall i,j,k,m. \tag{31}$$

The final step toward a convex reformulation is to convexify the *bilinear* term $g_{ijk}^{(ml)} = \nu_{ijk}^{(m)} \lambda_{ml}$ introduced in Lemma 5. For this purpose, we apply the special structured Reformulation-Linearization-Technique of Sherali *et al.* [21] to derive the following result (see [19, Appendix C] for proof details):

Lemma 6. *Given (28) with $\lambda_{ml} \in \{0,1\}$, $\forall m, l$, and given bounds $0 \leq \nu_{ijk}^{(m)} \leq \bar{\nu}_{ijk}^{(m)}$, the bilinear equation $g_{ijk}^{(ml)} = \nu_{ijk}^{(m)} \lambda_{ml}$ holds if and only if*

$$g_{ijk}^{(ml)} \geq 0, \quad g_{ijk}^{(ml)} - \bar{\nu}_{ijk}^{(m)} \lambda_{ml} \leq 0, \tag{32}$$

$$\sum_{l=1}^{F} g_{ijk}^{(ml)} - \nu_{ijk}^{(m)} = 0, \quad \forall i,j,k,m. \tag{33}$$

It is worth pointing out that Lemma 6 implies that (32) and (33) with the second constraint in (28) and $\lambda \geq 0$ effectively construct the *convex hull* of the bilinear relationship in $g_{ijk}^{(ml)}$. This allows for the tightest convex relaxation for the original problem and will significantly speed up the branch-and-bound process we propose later in Section V (see [19, Appendix C] for more detailed discussions).

Putting all the previous derivations together, we obtain the following equivalent reformulation of Problem FPPC (denoted as R-FPPC):

R-FPPC:

Min P

s.t. a) RLT reformulation for minimum received power constraints: $(27), (28), (31), (32), (33)$,

b) Distance reformulation constraints: $(22), (23), (24)$,

c) FBS association constraint: (11).

In R-FPPC, all constraints are either linear or convex, and so Problem R-FPPC is a *mixed-integer convex program* (MICP). Hence, it can readily be solved by a branch-and-bound (BB) process (see Section III) coupled with its convex relaxation. However, to design a more efficient and robust global optimization algorithm, in the next section, we will go one step further to simplify R-FPPC.

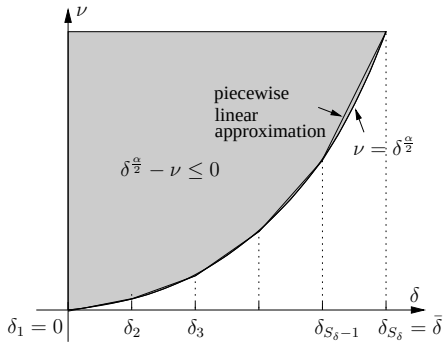

Fig. 4. An illustration of the piece-wise linear approximation for constraint $(\delta_{ijk}^{(m)})^{\frac{\alpha}{2}} - \nu_{ijk}^{(m)} \leq 0$ (dropping indices i, j, k, m for notational simplicity).

IV. Reformulation Step Two: Linearization of the Nonlinear Model

As mentioned earlier, although R-FPPC is an MICP and can be solved by BB, the convex relaxation of R-FPPC remains a nonlinear program, which in general may not be solved as efficiently as a linear program of similar size. This motivates us to consider approximating R-FPPC using a linear approximation, which further transforms the problem into a mixed-integer linear program (MILP). The fundamental rationale behind this approach is that MILP has been extensively explored by the operations research community for decades and powerful algorithms, techniques, and codes exist for solving large-scale problems [20].

More specifically, our approach is to use piecewise linear approximation (PLAP) functions to replace all nonlinear constraints in R-FPPC. To this end, let us first consider the convex constraint $(\delta_{ijk}^{(m)})^{\frac{\alpha}{2}} - \nu_{ijk}^{(m)} \leq 0$. For notational simplicity, we drop the indices i, j, k, and m and rewrite the constraint in the following form:

$$(\delta)^{\frac{\alpha}{2}} - \nu \leq 0. \tag{34}$$

Since we are only interested in values of δ over the interval $[0, \bar{\delta}]$, we can partition $[0, \bar{\delta}]$ into $S_\delta - 1$ smaller intervals via grid points $0 = \delta_1, \delta_2, \ldots, \delta_{S_\delta} = \bar{\delta}$, as shown in Fig. 4.[1] Intuitively, the accuracy of the approximation improves as the number of grid points increases. Indeed, it can be shown that the error introduced by PLAP is bounded and can be made arbitrarily small if the number of grid points goes to infinity [19]. In our numerical studies, we will also study the adequate number of grid points to achieve a close approximation.

Mathematically, the region obtained by replacing $(\delta)^{\frac{\alpha}{2}} - \nu \leq 0$ with PLAP can be written via the following linear constraints:

[1]Note that Fig. 4 is just for illustrative purposes and the grid points may or may not be equidistant, and different δ-variables may have different numbers of intervals.

$$\sum_{s=1}^{S_\delta} \tau_s (\delta_s)^{\frac{\alpha}{2}} - \nu \leq 0, \quad \sum_{s=1}^{S_\delta} \tau_s \delta_s = \delta, \text{ and } \sum_{s=1}^{S_\delta} \tau_s = 1, \quad (35)$$

where $\tau_s \geq 0$, for $s = 1, \ldots, S_\delta$ and *at most two* τ_s-variables are positive and they should be *adjacent*. However, noting that $\nu = (\delta)^{\frac{\alpha}{2}}$ is *strictly* convex for $\alpha > 2$, we can show that this adjacency requirement can be discarded as stated in the following proposition:

Proposition 7. *Consider the PLAP of Problem R-FPPC with constraints in (35). Then, for each constraint in the form of (34), at most two τ_s-variables are positive and they must be adjacent. Moreover, each $\delta = \sum_{s=1}^{S_\delta} \tau_s \delta_s$ is feasible to Problem R-FPPC.*

Proposition 7 can be proved by contradiction and exploiting the convexity of (34). Due to limited space, we relegate the details of the proof to [19, Appendix D].

Next, we construct a piecewise linear approximation for the nonlinear constraint $(X_{mi} + \frac{1}{2}\gamma_x)^2 + (Y_{mj} + \frac{1}{2}\gamma_y)^2 + (hz_m - ((k-1)h + \eta))^2 - \delta_{ijk}^{(m)} \leq 0$. We first expand this constraint as follows:

$$\begin{aligned} &B_{mi} + D_{mj} + h^2 E_m + \gamma_x X_{mi} + \gamma_y Y_{mj} \\ &\quad - 2h((k-1)h + \eta) z_m - \delta_{ijk}^{(m)} \\ &\quad \leq -\frac{1}{4}\gamma_x^2 - \frac{1}{4}\gamma_y^2 - ((k-1)h + \eta)^2, \end{aligned} \quad (36)$$

$$X_{mi}^2 - B_{mi} \leq 0,\ Y_{mj}^2 - D_{mj} \leq 0,\ z_m^2 - E_m \leq 0, \quad (37)$$

where we have again changed the equality relationships $B_{mi} = X_{mi}^2$, $D_{mj} = Y_{mj}^2$, and $E_m = z_m^2$ into inequality relationships based on the same reason as in Lemma 2. Then, we can use the identical PLAP technique for constraints in (37). To this end, let S_X, S_Y, and S_z denote the numbers of grid points for the X_{mi}–, Y_{mj}–, and z_m–variables, respectively, and let $X_{mi,1}, \ldots, X_{mi,S_X}$, $Y_{mj,1}, \ldots, Y_{mj,S_Y}$, and $z_{m,1}, \ldots, z_{m,S_z}$ denote the grid points for the X_{mi}–, Y_{mj}–, and z_m–variables, respectively. Let $\xi_{mi,1}^{(X)}, \ldots, \xi_{mi,S_X}^{(X)}$, $\xi_{mj,1}^{(Y)}, \ldots, \xi_{mj,S_Y}^{(Y)}$, and $\xi_{m,1}^{(z)}, \ldots, \xi_{m,S_z}^{(z)}$ denote the non-negative weights corresponding to the X_{mi}–, Y_{mj}–, and z_m–variables, respectively. Then, the PLAP for (37) are given as follows (dropping indices i, j, k and m for notational simplicity):

$$\sum_{s=1}^{S_X} \xi_s^{(X)} (X_s)^2 \leq B,\ \sum_{s=1}^{S_X} \xi_s^{(X)} (X_s) = X,\ \sum_{s=1}^{S_X} \xi_s^{(X)} = 1; \quad (38)$$

$$\sum_{s=1}^{S_Y} \xi_s^{(Y)} (Y_s)^2 \leq D,\ \sum_{s=1}^{S_Y} \xi_s^{(Y)} (Y_s) = Y,\ \sum_{s=1}^{S_Y} \xi_s^{(Y)} = 1; \quad (39)$$

$$\sum_{s=1}^{S_z} \xi_s^{(z)} (z_s)^2 \leq E,\ \sum_{s=1}^{S_z} \xi_s^{(z)} (z_s) = z,\ \sum_{s=1}^{S_z} \xi_s^{(z)} = 1. \quad (40)$$

Finally, replacing all nonlinear constraints in R-FPPC by the piecewise linear approximations in (35), (36), (38), (39), and (40), we have the final MILP problem as follows:

R-FPPC-MILP:

Min P

s.t. a) RLT reformulation for minimum received power constraints: $(28), (31), (32), (33)$,

b) PLAP for Constraint $(27) : (35)$,

c) PLAP for Constraint $(22) : (36), (38), (39), (40)$,

b) Absolute value reformulation constraints: $(23), (24)$,

e) FBS association constraint: (11).

V. A Solution Procedure Based on a Branch-and-Bound Framework and Linear Programming Relaxations

Using the two-step reformulations, we have arrived at an equivalent problem R-FPPC-MILP, which positions us to devise a solution procedure based on the branch-and-bound (BB) framework, which *guarantees* finding a global optimal solution [20]. In this section, we provide an overview on using BB to solve R-FPPC-MILP. For a comprehensive understanding of the BB procedure, we refer readers to [20] for more details.

The BB solution procedure proceeds iteratively as follows. For R-FPPC-MILP, during the initial step, a lower bound on the objective value is obtained by solving its linear programming relaxation (LPR). Because of the relaxation, the values of $\pi_{ijk}^{(m)}$ and λ_{ml} in the LPR solution are likely fractional. Thus, we conduct a local search (e.g., through judicious rounding) to recover a feasible solution from the LPR solution. This feasible solution provides an incumbent solution to R-FPPC-MILP and an upper bound on the objective value. Next, we branch the problem into two subproblems. The LPR of each of these two subproblems is then solved and local search is again used to obtain the lower and upper bounds. This step completes an iteration.

After an iteration, if the gap between the current upper bound and the smallest lower bound (among all the subproblems) is larger than some predefined desired error ϵ, we perform another iteration on the subproblem having the smallest lower bound. Also, during each iteration, we can remove those subproblems whose lower bounds have a gap less than ϵ compared to the global upper bound (since further branching on these subproblems could not yield improved feasible solutions), thus controlling the increase in the total number of subproblems in the system. The BB iterations continue until the smallest upper bound and the smallest lower bound among all the subproblems are within ϵ. Therefore, the best feasible solution is $(1-\epsilon)$-optimal. We summarize the BB/LPR procedure in Algorithm 1.

Finally, we point out that the BB/LPR algorithm can be used to determine the minimum required value of M to ensure coverage. For a given network, we can start from a small value, say $M = 1$ or 2. If M is not large enough, BB/LPR will detect the infeasibility of the underlying problem. Then, we can do a bisection search on M and repeat BB/LPR until the problem becomes feasible (i.e., of complexity $O(\log(\min\{M\}))$).

Algorithm 1 BB/LPR Solution Procedure

Initialization:

1. Let the optimal solution $\psi^* = \emptyset$ and the initial upper bound $UB = \infty$.
2. Let the initial problem list contain only the original problem, denoted by P_1.
3. Construct and solve the linear programming relaxation. Denote the solution to this relaxation as $\hat{\psi}_1$ and its objective value as the lower bound LB_1.

Main Loop:

4. Select a problem P_z that has the smallest lower bound (designated as LB) among all problems in the problem list.
5. Find, if necessary, a feasible solution ψ_z via a local search algorithm for Problem P_z. Denote the objective value of ψ_z by UB_z.
6. If $UB_z < UB$, then let $\psi^* = \psi_z$ and $UB = UB_z$. If $LB \geq (1-\epsilon)UB$ then stop with the $(1-\epsilon)$-optimal solution ψ^*; else, remove all problems $P_{z'}$ having $LB_{z'} \geq (1-\epsilon)UB$ from the problem list.
7. Select a binary variable (π or λ) and branch on the dichotomy of its value being 0 or 1.
8. Remove the selected problem P_z from the problem list, and construct two new problems P_{z1} and P_{z2} based on the foregoing branching step.
9. Compute two new lower bounds LB_{z1} and LB_{z2} by solving the linear programming relaxations of P_{z1} and P_{z2}, respectively.
10. If $LB_{z1} < (1-\epsilon)UB$ then add Problem P_{z1} to the problem list. If $LB_{z2} < (1-\epsilon)UB$ then add Problem P_{z2} to the problem list.
11. If the problem list is empty, stop with the $(1-\epsilon)$–optimal solution ψ^*. Otherwise, go to Step 4.

VI. Numerical Results

In this section, we conduct numerical studies to demonstrate the efficacy of our proposed optimization approach. First, we use a building with 36 subregions as an example. As shown in Fig. 5, the building's length, width, and floor height are 100, 60, and 3 meters, respectively. The occupant probabilities are listed in Table I and also illustrated in Fig. 5: the darker a subregion, the higher its occupant probability. The transmission power limit of each handset is 1 W. The minimum received power threshold for each handset is -80 dBm. The path loss exponent is 3.5. The shadowing effect deviation is 5 dB. Using our proposed optimization approach, the maximum weighted transmission power of the handsets is minimized to 0.0028 W. As shown in Fig. 5, the optimal FBS locations are: FBS1: $(x_1 = 87.5, y_1 = 30.2, z_1 = 3)$, FBS2: $(x_2 = 24.7, y_2 = 30.7, z_2 = 3)$, FBS3: $(x_3 = 75.7, y_3 = 30.8, z_3 = 2)$, FBS4: $(x_4 = 22.8, y_4 = 28.1, z_4 = 2)$, FBS5: $(x_5 = 66.8, y_5 = 19.9, z_5 = 1)$, and FBS6: $(x_6 = 13.1, y_6 = 31.2, z_6 = 1)$. The optimal association relationship for each subregion is also shown in Fig. 5. As expected, due to FAF effect, not all subregions are associated with its closest FBS.

For our proposed PLAP technique, it is interesting to see how many grid points are needed to achieve a close approximation to the original R-FPPC problem. For the network in Fig. 5, we adopt the following rule for the grid point values: $S_X = S_Y = S_z = S$ and $S_\delta = 10S$. We vary S from 2 (i.e., no intermediate grid point) to 40 and the results are shown in Fig. 6. We can see that, as S increases, the PLAP objective value rapidly converges to the original problem. In this example, the PLAP objective value is near optimal when $S \geq 10$. Hence, in the subsequent numerical studies, we set $S = 40$, which guarantees a negligible approximation error almost surely.

TABLE I
THE OCCUPANT PROBABILITIES OF THE 36 SUBREGIONS IN FIG. 5.

(i,j,k)	q_{ijk}	(i,j,k)	q_{ijk}	(i,j,k)	q_{ijk}
$(1,1,1)$	0.047	$(1,1,2)$	0.058	$(1,1,3)$	0.002
$(1,2,1)$	0.027	$(1,2,2)$	0.011	$(1,2,3)$	0.008
$(1,3,1)$	0.024	$(1,3,2)$	0.040	$(1,3,3)$	0.034
$(2,1,1)$	0.026	$(2,1,2)$	0.037	$(2,1,3)$	0.032
$(2,2,1)$	0.050	$(2,2,2)$	0.064	$(2,2,3)$	0.001
$(2,3,1)$	0.001	$(2,3,2)$	0.033	$(2,3,3)$	0.009
$(3,1,1)$	0.020	$(3,1,2)$	0.045	$(3,1,3)$	0.003
$(3,2,1)$	0.031	$(3,2,2)$	0.014	$(3,2,3)$	0.003
$(3,3,1)$	0.033	$(3,3,2)$	0.031	$(3,3,3)$	0.018
$(4,1,1)$	0.050	$(4,1,2)$	0.001	$(4,1,3)$	0.031
$(4,2,1)$	0.007	$(4,2,2)$	0.057	$(4,2,3)$	0.043
$(4,3,1)$	0.012	$(4,3,2)$	0.054	$(4,3,3)$	0.046

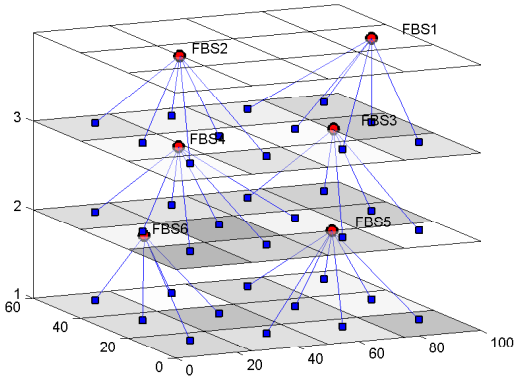

Fig. 5. The optimal FBS locations and the association relationship for each subregion in a 20-subregion building.

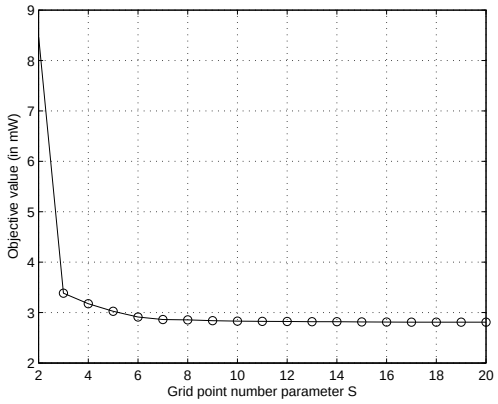

Fig. 6. The objective value with PLAP converges as the grid point number parameter S increases.

Next, we examine the efficiency and the scaling of the running time of our proposed algorithm as the number of subregions increases. The size of the building and wireless channel/transceivers parameters are the same as in the previous example. We increase the number of subregions as follows: 6 $(2 \times 1 \times 3)$, 12 $(2 \times 2 \times 3)$, 18 $(3 \times 2 \times 3)$, 24 $(4 \times 2 \times 3)$, 30 $(5 \times 2 \times 3)$, and 36 $(4 \times 3 \times 3)$. For each setting, the runtime is obtained by averaging over 50 randomly generated examples. The results are shown in Fig. 7, which depicts the y-axis in both linear and log scale. For comparative purposes,

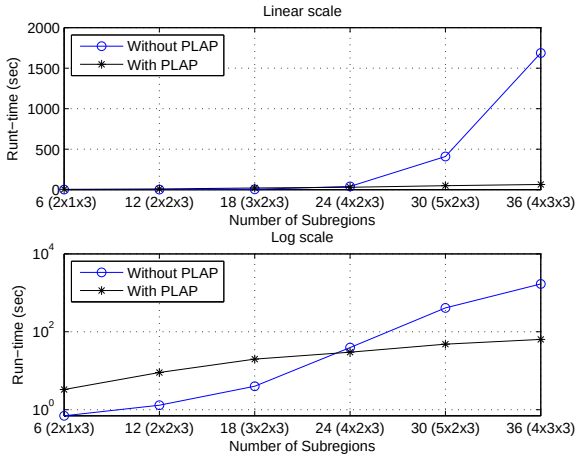

Fig. 7. The scaling of run-time with respect to the number of subregions.

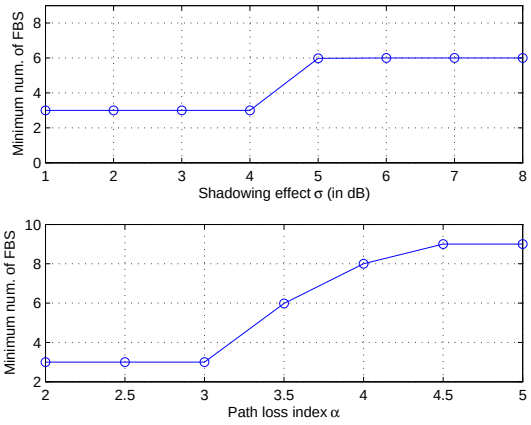

Fig. 8. The scaling of minimum number of FBSs for network coverage as the path loss exponent and the shadowing effect deviation grow.

we plot the BB run-time with and without PLAP. In both cases, the run-time increases roughly exponentially, which is an expected phenomenon when searching for global optimal solutions for mixed-integer programs. However, it can be seen that with PLAP, the increase of run-time is much slower than that without PLAP. This exhibits the beneficial effect of our proposed PLAP approach.

As mentioned earlier, our BB/LPR algorithm can also be used to determine the minimum required number of FBSs to ensure network coverage. As an example, here we study how the minimum required number of FBSs changes as the wireless channel parameters vary. Again, the size of the buildings used in this simulation remains the same as before. We study two settings: 1) fix the path loss exponent α to 3.5 and vary the shadowing effect deviation σ from 1 dB to 8 dB (i.e., channels fluctuate more and more); and 2) fix the shadowing effect deviation σ to 5 dB and vary the path loss exponent from 2 to 5 (i.e., signals attenuate faster and faster). For each case, the result is obtained by averaging over 50 randomly generated examples. The results are shown in Fig. 8. We can see that when σ varies from 1 dB to 8 dB, the minimum required number of FBSs increases from 3 to 6. Likewise, when α increases from 2 to 5, the minimum required number of FBSs increases from 3 to 9.

VII. Conclusion

In this paper, we studied a joint femtocell base station (FBS) placement and power control optimization problem for commercial buildings with the aim to prolong mobile handsets' battery lives. We constructed a mathematical model that considers the floor attenuation factor and FBS location restrictions in building environments. Based on this model, we proposed a novel two-step reformulation technique to transform the original mixed-integer nonconvex problem into a mixed-integer linear program. This reformulation technique led to an efficient global optimization algorithm based on a branch-and-bound framework with linear programming relaxations, which *guarantees* finding a global optimal solution. Moreover, our numerical studies showed that the run-time for the proposed algorithm scales slowly with respect to the number of subregions in a building. We note that femtocell placement in commercial buildings is an important and yet under-explored area. This paper offers both useful theoretical insights and practical design tools for future femtocell planning in commercial buildings. Possible future directions include to study the placement problem in two-tier femtocell networks, to consider joint spectral management and placement optimization, and to develop fast approximation algorithms with provable performance guarantees (e.g., constant-factor approximation).

Appendix A
Proof of Lemma 1

Combining (2) and (4) and noting that the number of floors between the subregion (i,j,k) and the m-th FBS is $|z_m - w|$, we obtain that (in dBm)

$$P_{R_m} = \begin{cases} P_{ijk} - L_{d_0} - 10\alpha \log_{10}\left(\frac{d_{ijk}^{(m)}}{d_0}\right), & \text{if } z_m = k, \\ P_{ijk} - L_{d_0} - 10\alpha \log_{10}\left(\frac{d_{ijk}^{(m)}}{d_0}\right) & \\ \qquad -\Delta_1 - (|z_m - k| - 1)\Delta_a, & \text{if } z_m \neq k. \end{cases}$$

This implies that, after converting each of P_{R_m}, P_{ijjk}, and L_{d_0} to a linear scale (i.e., letting $y = 10^{\frac{x}{10}}$, where x and y are in dBm and the linear scale, respectively), we have

$$P_{R_m} = \begin{cases} \frac{P_{ijk}}{L_{d_0}(d_{ijk}^{(m)}/d_0)^{\alpha}}, & \text{if } z_m = k, \\ \frac{P_{ijk}}{L_{d_0}(d_{ijk}^{(m)}/d_0)^{\alpha} 10^{(\Delta_1/10)} 10^{((|z_m - k| - 1)\Delta_a/10)}} & \text{if } z_m \neq k. \end{cases} \tag{41}$$

Then, the result in (5) follows by letting $C_0 = L_{d_0} d_0^{-\alpha}$, $C_1 = L_{d_0} d_0^{-\alpha} 10^{(\Delta_1 - \Delta_a)/10}$, and $\Delta = 10^{\Delta_a/10}$. □

APPENDIX B
PROOF OF LEMMA 5

Since z_m is integer-valued on $\{1,\ldots,F\}$, we can rewrite it as the following equivalent binary representation:

$$z_m = \sum_{l=1}^{F} l\lambda_{ml}, \quad \forall m,$$

where $\lambda_{ml} \in \{0,1\}$, $\forall m,l$, such that

$$\sum_{l=1}^{F} \lambda_{ml} = 1, \quad \forall m.$$

As a result, we can reformulate the nonconvex constraint $\mu_{mk} = \Delta^{|z_m-k|}$ in (26) as the following *linear* constraint in the λ_{ml}-variables.

$$\mu_{mk} = \sum_{l=1}^{F} \lambda_{ml}\Delta^{|l-k|}, \quad \forall m,k. \tag{42}$$

With (42), we can further simplify (26) into an expression that only involves binary variables instead of general integer variables. Substituting (42) into the first constraint in (26), the latter becomes:

$$A(z_m,k)\sum_{l=1}^{F}\Delta^{|l-k|}\nu_{ijk}^{(m)}\lambda_{ml} - (1-\pi_{ijk}^{(m)})U_{ijk}^{(m)} - P_{ijk} \le 0, \quad \forall i,j,k,m. \tag{43}$$

Recall that $A(z_m,k)$ is equal to A_0 if $z_m = k$ and equals A_1 if $z_m \neq k$. Thus, (43) can be further written as

$$A_1\sum_{l=1,l\neq k}^{F}\Delta^{|l-k|}\nu_{ijk}^{(m)}\lambda_{ml} + A_0\nu_{ijk}^{(m)}\lambda_{mk} - (1-\pi_{ijk}^{(m)})U_{ijk}^{(m)} - P_{ijk} \le 0, \quad \forall i,j,k,m. \tag{44}$$

So far, we have converted the highly unstructured expression in (15) to an expression in (44) that is linear in the binary variables $\pi_{ijk}^{(m)}$, but has *bilinear* terms $\nu_{ijk}^{(m)}\lambda_{ml}$. Then, by letting

$$g_{ijk}^{(ml)} \triangleq \nu_{ijk}^{(m)}\lambda_{ml}, \quad \forall i,j,k,m,l, \tag{45}$$

we can see that (44) can be linearized as

$$A_1\sum_{l=1,l\neq k}^{F}\Delta^{|l-k|}g_{ijk}^{(ml)} + A_0 g_{ijk}^{(ml)} - (1-\pi_{ijk}^{(m)})U_{ijk}^{(m)} - P_{ijk} \le 0, \quad \forall i,j,k,m.$$

This completes the proof.

APPENDIX C
PROOF OF LEMMA 6

We first show the "only if" part. Since $\nu_{ijk}^{(m)}$ is non-negative and bounded from above and λ_{ml} is binary, we have

$$\nu_{ijk}^{(m)} \ge 0, \quad \nu_{ijk}^{(m)} - \bar{\nu}_{ijk}^{(m)} \le 0, \quad \text{and} \quad \lambda_{mk} \ge 0, \tag{46}$$

in addition to (29), where $\bar{\nu}_{ijk}^{(m)}$ denotes an upper bound for $\nu_{ijk}^{(m)}$. From the inequalities in (46), we derive the following two so-called bound-factor constraints:

$$\nu_{ijk}^{(m)}\lambda_{ml} \ge 0, \quad \text{and} \quad (\nu_{ijk}^{(m)} - \bar{\nu}_{ijk}^{(m)})\lambda_{ml} \le 0,$$

which, upon applying the substitution (45), yields:

$$g_{ijk}^{(ml)} \ge 0, \quad \text{and} \quad g_{ijk}^{(ml)} - \bar{\nu}_{ijk}^{(m)}\lambda_{ml} \le 0.$$

Furthermore, multiplying both sides of (29) by $\nu_{ijk}^{(m)}$ and using (45), we derive:

$$\sum_{l=1}^{F} g_{ijk}^{(ml)} - \nu_{ijk}^{(m)} = 0, \quad \forall i,j,k,m.$$

This completes the proof of the "only if" part of the theorem.

Conversely, note that when $\lambda_{ml} = 0$, then (32) implies that $g_{ijk}^{(ml)} = 0 = \nu_{ijk}^{(m)}\lambda_{ml}$. On the other hand, when $\lambda_{ml} = 1$, it follows from (29) that $\lambda_{ml'} = 0$, $\forall l' \neq l$. As above, we have $g_{ijk}^{(ml')} = 0$, $\forall l' \neq l$. Thus, we obtain that $g_{ijk}^{(ml)} = \nu_{ijk}^{(m)} = \nu_{ijk}^{(m)}\lambda_{ml}$, using (33) along with $g_{ijk}^{(ml')} = 0$, $\forall l' \neq l$. This completes the proof of "if" part of the theorem.

APPENDIX D
PROOF OF PROPOSITION 7

Without loss of generality, suppose that there J constraints in the form of (34). Thus, we have the following PLAP constraints:

$$\sum_{s=1}^{S_\delta}\tau_{js}(\delta_{js})^{\frac{\alpha}{2}} - \nu_j \le 0, \quad j = 1,\ldots,J,$$
$$\sum_{s=1}^{S_\delta}\tau_{js} = 1,\ j = 1,\ldots,J, \quad \tau_{js} \ge 0, \text{ for } s = 1,\ldots,S_\delta,$$

To prove the first part of Proposition 7, it suffices to show that if τ_{js_1} and τ_{js_2} are positive, the grid points δ_{js_1} and δ_{js_2} must be adjacent. By contradiction, suppose that there are τ_{js_1} and $\tau_{js_2} > 0$ such that they are not adjacent. Then, there exists a grid point $\delta_{js'} \in (\delta_{js_1}, \delta_{js_2})$ such that $\delta_{js'} = \mu_{j1}\delta_{js_1} + \mu_{j2}\delta_{js_2}$, where $\mu_{j1},\mu_{j2} > 0$ and $\mu_{j1} + \mu_{j2} = 1$. Next, for the optimal solution to the PLAP of R-FPPC, let $\rho_j \ge 0$ be the optimum Lagrangian multipliers associated with the constraint $\sum_{s=1}^{S_\delta}\tau_{js}(\delta_{js})^{\frac{\alpha}{2}} - \nu_j \le 0$ and let θ_j be the optimal Lagrangian multiplier associated with the constraint $\sum_{s=1}^{S_\delta}\tau_{js} = 1$. Then, it is easy to verify that the following subset of the KKT conditions holds:

$$\rho_j((\delta_{js_1})^{\frac{\alpha}{2}} - \nu_j) + \theta_j = 0, \tag{47}$$
$$\rho_j((\delta_{js_2})^{\frac{\alpha}{2}} - \nu_j) + \theta_j = 0, \tag{48}$$
$$\rho_j((\delta_{js})^{\frac{\alpha}{2}} - \nu_j) + \theta_j = 0, \forall s. \tag{49}$$

Now, we show that the last condition in (49) is contradicted for $s = s'$. By the strict convexity of $\delta^{\frac{\alpha}{2}} - \nu$, we have

$$\begin{aligned}
&\rho_j((\delta_{js'})^{\frac{\alpha}{2}} - \nu_j) + \theta_j \\
&= \rho_j((\mu_{j1}\delta_{js_1} + \mu_{j2}\delta_{js_2})^{\frac{\alpha}{2}} - \nu_j) + \theta_j \\
&< \rho_j(\mu_{j1}((\delta_{js_1})^{\frac{\alpha}{2}} - \nu_j) + \mu_{j2}((\delta_{js_2})^{\frac{\alpha}{2}} - \nu_j) + \theta_j \\
&= \mu_{j1}\Big(\rho_j((\delta_{js_1})^{\frac{\alpha}{2}} - \nu_j) + \theta_j\Big) + \\
&\quad \mu_{j2}\Big(\rho_j((\delta_{js_2})^{\frac{\alpha}{2}} - \nu_j) + \theta_j\Big) = 0.
\end{aligned}$$

This contradicts (49) for $s = s'$, and hence, δ_{js_1} and δ_{js_2} must be adjacent, i.e., the first part of Proposition 7 is proved.

To show the second part of Proposition 7, by the convexity of $\delta^{\frac{\alpha}{2}} - \nu_j$, we have

$$\delta^{\frac{\alpha}{2}} - \nu_j = \Big(\sum_{s=1}^{S_\delta} \tau_{js}\delta_{js}\Big)^{\frac{\alpha}{2}} - \nu_j \leq \sum_{s=1}^{S_\delta} \tau_{js}\Big((\delta_{js})^{\frac{\alpha}{2}} - \nu_j\Big) \leq 0.$$

Hence, $\delta = \sum_{s=1}^{S_\delta} \tau_{js}\delta_{js}$ is feasible and the proof is complete.

REFERENCES

[1] "Presentations by ABI Research, Picochip, Airvana, IP.access, Gartner, Telefonica Espana," 2nd Int'l. Conf. Home Access Points and Femtocells, 2007. [Online]. Available: http://www.avrenevents.com/dallas-femto2007/purchase_presentations.htm

[2] V. Chandrasekhar, M. Kountouris, and J. G. Andrews, "Coverage in multi-antenna two-tier networks," *IEEE Trans. Wireless Commun.*, vol. 8, no. 10, pp. 5314–5327, Oct. 2009.

[3] I. Ashraf, H. Claussen, and L. T. Ho, "Distributed radio coverage optimization in enterprise femtocell networks," in *Proc. IEEE International Conference on Communications (ICC)*, Cape Town, South Africa, May 23-27, 2010, pp. 1–6.

[4] O. Simeone, E. Erkip, and S. Shamai (Shitz), "Robust transmission and interference management for femtocells with unreliable network access," *IEEE J. Sel. Areas Commun.*, vol. 28, no. 9, pp. 1469–1478, Dec. 2010.

[5] V. Chandrasekhar and J. G. Andrews, "Uplink capacity and interference avoidance for two-tier femtocell networks," *IEEE Trans. Wireless Commun.*, vol. 8, no. 7, pp. 3498–3509, Jul. 2009.

[6] H.-S. Jo, C. Mun, J. Moon, and J.-G. Yook, "Interference mitigation using uplink power control for two-tier femtocell networks," *IEEE Trans. Wireless Commun.*, vol. 8, no. 10, pp. 4906–4910, Oct. 2009.

[7] Y. J. Sang, H. G. Hwang, and K. S. Kim, "A self-organized femtocell for IEEE 802.16e system," in *Proc. IEEE Globecom*, Honolulu, HI, Nov.30–Dec.04, 2009, pp. 1–5.

[8] H.-S. Jo, C. Mun, J. Moon, and J.-G. Yook, "Self-optimized coverage coordination in femtocell networks," *IEEE Trans. Wireless Commun.*, vol. 9, no. 10, pp. 2977–2982, Oct. 2010.

[9] P. Xia, V. Chandrasekhar, and J. G. Andrews, "Open vs. closed access femtocells in the uplink," *IEEE Trans. Wireless Commun.*, vol. 9, no. 12, pp. 3798–3809, Dec. 2010.

[10] D. Choi, P. Monajemi, S. Kang, and J. Willasenor, "Dealing with loud neighbors: The benefits and tradeoffs of adaptive femtocell access," in *Proc. IEEE Globecom*, New Orleans, LA, Nov.30–Dec.4, 2008, pp. 1–5.

[11] V. Chandrasekhar, J. G. Andrews, and A. Gatherer, "Femtocell networks: A survey," *IEEE Commun. Mag.*, vol. 46, no. 9, pp. 59–67, Sep. 2008.

[12] R. Y. Kim, J. S. Kwak, and K. Etemad, "WiMAX femtocell: Requirements, challenges, and solutions," *IEEE Commun. Mag.*, vol. 47, no. 9, pp. 84–91, Sep. 2009.

[13] C. Patel, M. Yavuz, and S. Nanda, "Femtocells: Industry perspectives," *IEEE Wireless Commun. Mag.*, vol. 17, no. 5, pp. 6–7, Oct. 2010.

[14] "Smartphone review," TopTen Reviews, 2011. [Online]. Available: http://cell-phones.toptenreviews.com/smartphones/

[15] "Cell phone battery chart," CNET, 2010. [Online]. Available: http://reviews.cnet.com/cell-phone-battery-life-charts/?tag=leftNav.0

[16] T. S. Rappaport, *Wireless Communications: Principles and Practice*. Upper Saddle River, NJ: Prentice Hall, 2002.

[17] S. Seidel, T. Rappaport, M. Feuerstein, K. Blackard, and L. Grindstaff, "The impact of surrounding buildings on propagation for wireless in-building personal communications system design," in *Proc. IEEE VTC*, Denver, CO, May 10–13 1992, pp. 814–815.

[18] S. Y. Seidel and T. S. Rappaport, "914 MHz path loss prediction models for indoor wireless communications in multifloored buildings," *IEEE Trans. Antennas Propag.*, vol. 40, no. 2, pp. 207–217, Feb. 1992.

[19] J. Liu, Q. Chen, and H. D. Sherali, "Algorithm design for femtocell base station locations in commercial building environments," *Technical Report, Department of ECE, Ohio State University*, Jul. 2011. [Online]. Available: http://www2.ece.ohio-state.edu/~liu/publications/OPT_FBS_Loc.pdf

[20] G. L. Nemmhauser and L. A. Wolsey, *Integer and Combinatorial Optimization*, 2nd ed. New York: Wiley-Interscience Publication, 1999.

[21] H. D. Sherali, W. P. Adams, and P. J. Driscoll, "Exploiting special structures in constructing a hierarchy of relaxations for 0-1 mixed integer problems," *Operations Research*, vol. 46, no. 3, pp. 396–405, May 1998.